

Elastoplastic Modelling of Cyclic Shear Deformation of Amorphous Solids

Pushkar Khandare¹ and Srikanth Sastry^{1,*}

¹*Jawaharlal Nehru Centre for Advanced Scientific Research, Jakkur Campus, Bengaluru, 560064, India*

We develop an energy-landscape based elasto-plastic model to understand the behaviour of amorphous solids under uniform and cyclic shear. Amorphous solids are modeled as being composed of mesoscopic sub-volumes, each of which may occupy states - termed mesostates - drawn from a specified distribution. The energies of the mesostates under stress free conditions determine their stability range with respect to applied strain, and their plastic strain, at which they are stress free, forms an important additional property. Under applied global strain, mesostates that reach their stability limits transition to other permissible mesostates. Barring such transitions, which encompass plastic deformations that the solid may undergo, mesostates are treated as exhibiting linear elastic behavior, and the interactions between mesoscopic blocks are treated using the finite element method. The model reproduces known phenomena under uniform and cyclic shear, such as the brittle-to-ductile crossover with annealing and the Bauschinger effect for uniform shear, qualitative features of the yielding diagram under cyclic shear including the change in yielding behaviour with the degree of annealing, across a ‘threshold level’, and dynamic phenomena such as the divergence of failure times on approach to the yield point and the non-monotonic evolution of the local yield rate. In addition to these results, we discuss the dependence of the observed behaviour on model choices, and open questions highlighted by our work.

Introduction — Amorphous materials, which comprise of soft solids like gels, foams [1] and hard solids like metallic glasses [2, 3] show a rich phenomenology when subject to applied stress or deformation. Subjected to uniform shear deformation, amorphous materials show solid-like elastic response which is punctuated by stress drops as deformation progresses, eventually leading to material failure [4–8]. The yield process can be catastrophic, with a stress overshoot and subsequent localisation of strain, termed as shear banding [9], or gradual and homogeneous without a stress overshoot [6]. The nature of yielding depends on preparation history [10–12] (rapidly cooled glasses show ductile behavior, while slowly cooled glasses display a stress overshoot) and on the rate of deformation [13–16]. The yielding transition of glasses under cyclic shear [17–34] reveals a richer phenomenology. It was shown that the yielding transition is discontinuous, in the athermal quasistatic (AQS) limit, irrespective of the preparation history [20, 21, 25], and that the time taken to reach the final state appears to diverge on approaching the yielding transition amplitude from either side [18, 20, 21, 31–33]. Particularly striking is the emergence of a threshold energy wherein samples with inherent structure (IS) energies above and below this threshold (termed *poorly* and *well* annealed respectively) show qualitatively different yielding behaviour; and that the threshold energy corresponds to the temperature where a dynamical cross-over is observed [25]. Failure under cyclic deformation occurs *via* the formation of a shear band irrespective of the annealing level of the sample [22, 25], and samples show non-monotonic evolution of energies and local yield rate *en route* to failure [22, 29, 33, 34]. At low values of cyclic shear amplitude poorly annealed samples evolve towards absorbing states with lower energy, with all poorly annealed sam-

ples reaching a universal state termed the threshold state at a common yield amplitude. Beyond this amplitude the poorly annealed samples yield, with all samples tracing the same energy *vs.* strain amplitude curve, post-yield. Well annealed samples show negligible response to cyclic shear till a critical amplitude (greater than the yield amplitude of poorly annealed samples) is crossed, beyond which they follow the master curve that defines the universal yielded state that does not possess memory of the initial state. The deeper the annealing level below the threshold, higher is its critical amplitude.

The localized nature of plastic events in amorphous solids [4, 5] has prompted development of elasto-plastic models (EPMs, see [35] for a comprehensive review) which regard an amorphous solid to be composed of mesoscopic blocks that are coupled elastically. When the local stress (equivalently, strain) exceeds the local yield value, a plastic rearrangement occurs whereby the mesoscopic block experiences a stress drop, and a transition into a new local state. This new local state is characterised by a new plastic strain. Although many EPMS have been investigated using a single local yield stress value, those EPMS (and corresponding mean field treatments) aiming to incorporate the heterogeneity of amorphous solids consider a a distribution both of the local yield stress values, and the plastic strain increments [29–31, 36, 37].

With the aim of capturing the annealing and rejuvenation effects observed under cyclic shear, here we develop an EPM based on an energy landscape picture that represents the state of each mesoscopic region with so-called mesostates [27, 38]. Each mesostate is a set of stable configurations that can be continuously transformed into each other *via* changes in strain, within a stability range in strain values. Each unstrained mesostate

may be viewed as a local energy minimum (or inherent structure) of the mesoscopic block, with a corresponding density of states (DOS) we specify. Reaching either limit (we consider a scalar strain variable here) of the stability range will lead to a discontinuous transition to a new mesostate. It has been observed [25] in simulations that the stability range of deeper lying mesostates was larger in simple model glasses (see [39] for variations associated with the fragility of the corresponding glass formers), which we incorporate in our model. To complete the prescription we need to specify how the plastic strain increment is chosen. A single site model with these ingredients [27] captures several features of cyclic shear yielding, and has been the basis for further theoretical analysis of yielding and fatigue failure [28, 29, 34]. In the present work, we construct an EPM with the properties of a mesoscopic blocks as described above, whose elastic interactions are treated employing the finite element method (FEM), following previous work [40, 41]. A popular alternative approach [42, 43] uses the response of an infinite homogeneous elastic medium to a point plastic strain, which is then adapted to a finite periodic system, while others [30, 44, 45] account for the elastoplastic response by assuming a local disordered potential (with homogeneous elastic constants) with multiple minima.

The FEM approach treats the plastic strain to involve an extended region, as opposed to a point, and easily permits incorporation of heterogeneous elastic moduli. The computational cost in the homogeneous case is comparable to applying the analytically derived kernel, as the FEM response needs to be calculated only once for a unit plastic strain and the response to any given plastic strain field is then found by linear superposition. Our work is closely related to a recent investigation on cyclic shear phenomena using energy landscape based approaches [30, 31]. We systematically tune the model parameters, specifically the density of states and the plastic strain increment choice, and find a somewhat surprising sensitivity to specific choices. In addition to reproducing the phenomenology reported in earlier related works [30, 31], our results also show: i) the possibility of *trenching*, depending on model parameters, where the shear bands remain pinned for indefinite number of shear cycles, ii) non-monotonic evolution of the energy and local yield rate in the yielded regime, and iii) divergence of number of cycles needed to form a shear band, which are consistent with simulation results. Further, our work highlights the presence of an *intermediate* regime around yielding as a new feature, that needs further investigations to elucidate.

Model — A scalar single site model was previously introduced [27] which prescribes an energy landscape that is available to a single mesoscopic region undergoing shear deformation. Each region, hereafter termed mesoblock, shows linear elastic response around a stress-free plastic strain. The energy E_{0i} at the plastic strain

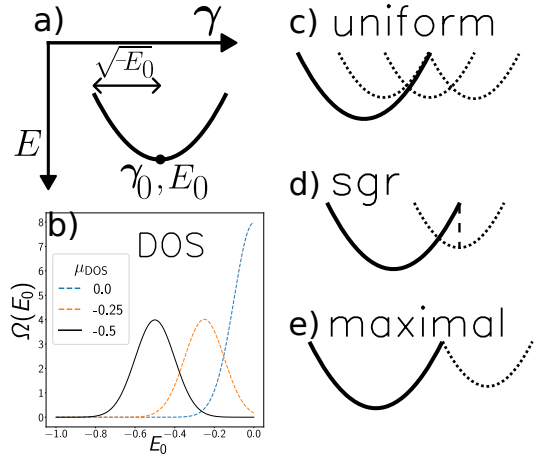


FIG. 1. (a) A single mesostate with energy $E(\gamma) = E_0 + \frac{\mu}{2}(\gamma - \gamma_0)^2$ is stable over a finite range in strain, $\gamma \in (\gamma_0 - \sqrt{-E_0}, \gamma_0 + \sqrt{-E_0})$. (b) Three choices of Gaussian density of states are shown, with the standard deviation fixed at 0.1. (c,d,e) Plastic strain increment rules. For the results in the main text the model choices are: $\mu_{DOS} = -0.5$ and *maximal* plastic increment.

γ_{0i} , and a stability range around the plastic strain state characterise the full mechanical behaviour of a mesoblock i . The elastic energy of a mesoblock thus reads, $E_i = E_{0i} + \frac{\mu}{2}(\gamma_i - \gamma_{0i})^2$, and we assume that deeper lying mesostates have a larger stability range, specifically, a mesoblock i is stable if $\gamma_i \in [\gamma_{0i} - \sqrt{-E_{0i}}, \gamma_{0i} + \sqrt{-E_{0i}}]$. Once the current mesoblock becomes unstable the E_0 value of the new mesostate is taken from a density of states of energy minima $\Omega(E_0)$. E_0 values are chosen to lie in the range $(-1, 0)$. We choose $\Omega(E_0)$ to be a Gaussian with mean -0.5 and standard deviation 0.1 . Transition to another mesostate is made with the constraint that the local elastic energy be lower at that local strain value, which implements the athermal protocol. The plastic strain value of the new mesostate can be chosen *via* any of the three protocols sketched in Fig. 1: uniform, soft glassy rheology (SGR) and maximal. The uniform choice consists of choosing with uniform probability a γ_0 such that the new mesostate is stable at that strain value, while the SGR choice sets the new plastic strain to be the current local γ_i . It was shown [27] that the single-site yielding diagram is robust to these two choices, giving qualitatively similar phenomenology. Here we use the *maximal* protocol employed in [30] where the new plastic strain is maximally away from the current plastic strain. The model we investigate consists of $L \times L$ mesoblocks coupled elastically, with the elastic couplings treated using the finite element method. We prepare samples of different degrees of annealing by first deriving the analytical occupation probability $P(E_0, T_p)$ of mesostate minima given a parent temperature T_p , and use a zero-mean Gaussian distribution of initial plastic

strains that gets narrower as T_p decreases. Details of the implementation and additional results, including the dependence on choice of model features, are given in the Supplemental Material (SM) [46].

Results: Uniform Shear — Uniform shear deformation (see Fig. 2a) reveals a ductile to brittle crossover as the parent temperature (T_p) is lowered. At large values of the strain (γ) all samples reach a common steady state stress value, $\sigma_{SS} = 0.737$, while the corresponding $\langle E_0 \rangle$ values reach a common value of -0.525 . Note that this is lower than the peak of the DOS since the stability range increases as E_0 decreases which induces a bias to the negative side of the peak of the DOS. Poorly annealed samples (that is, samples with higher T_p) exhibit ductile behaviour and reach this common $\langle E_0 \rangle$ value much faster than the brittle samples. This is because poorly annealed samples display system-wide homogeneous plastic activity. The steady state solid resembles a high temperature system. This is evidenced from the invariant distribution (of E_0) that is reached in the flow stress regime, see Fig. 2b. The distribution mimics that of a system corresponding to $T_p = 0.4$ [46]. Well annealed samples, on the other hand, fail with a stress overshoot followed by a stress drop, with the plastic activity being confined to a banded region which is termed as a *shear band*. This band grows with increasing strain (inset of Fig. 2d), with a square root growth law [46]; this slow growth is captured in the E_0 evolution as well. Once this shear band has grown to the linear extent of the system we expect total erasure of initial conditions.

The Baushchinger effect is an example of mechanical memory where we observe a softening of the response in the direction opposite to that in which the sample was previously deformed [47–49]. When we probe the response of a freshly prepared sample to shear strain in either direction, the response is found to be isotropic, see Fig. 2e. However when the sample is sheared in the positive direction and the strain is reversed till the stress is zero (see inset, 2e), there is a change – The response in the direction opposite to the initial loading is softer, see Fig. 2e. In Fig. 2f we plot the distribution of distance to the respective stability thresholds (γ^+ for forward, and γ^- for reverse loading) for the fresh and the pre-sheared samples. The distributions in either direction are equivalent for the fresh sample while the distribution of forward distances are severely depleted in the low x regime for the pre-sheared sample. This is due to a progressive removal of low x sites during the preparation of pre-sheared sample as reported previously in [43].

Cyclic Shear — In Fig. 3a we plot the evolution of the stroboscopic mesostate energy E (at the end of each cycle, at zero strain) for a poorly annealed sample ($T_p = 3.16$). For driving amplitude $\gamma_{max} \leq \gamma_{max}^{yield}$ ($= 0.43$), we see that the energy drops with number of cycles and reaches an absorbing state. For higher values of γ_{max} we observe initial annealing not unlike the evo-

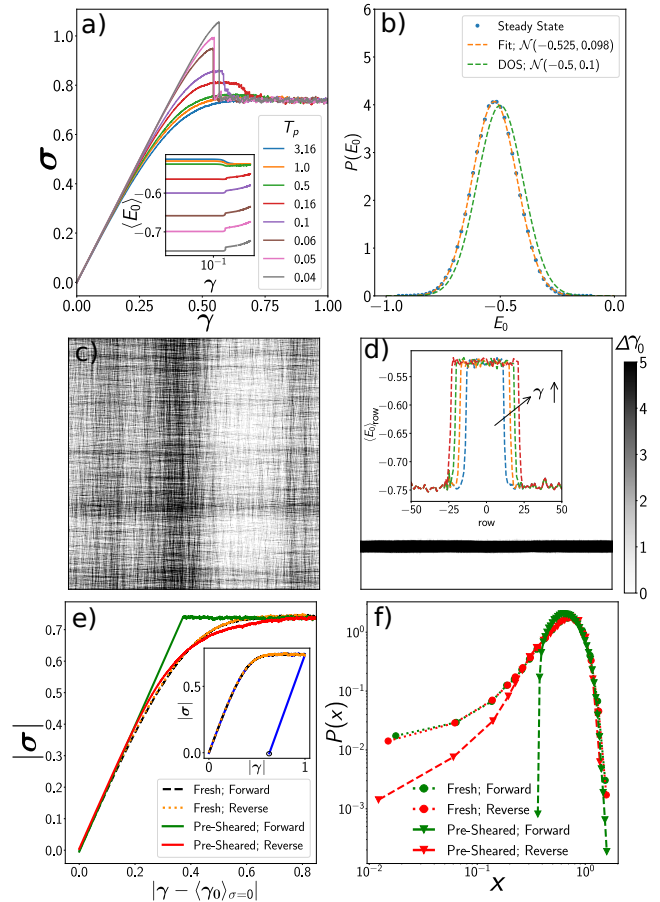


FIG. 2. (a) The stress σ is plotted for strain-controlled uniform deformation for various annealing levels as indicated by the parent temperature T_p . (Inset) Energy E_0 evolution is plotted. (b) Distribution of local E_0 in the steady state is plotted with blue points and dashed orange line denotes a Gaussian distribution with mean -0.525 and standard deviation 0.098 . The density of states is plotted for comparison. (c,d) The change in the plastic strain field between configurations at $\gamma = 2.0$ and $\gamma = 4.0$ is plotted for (c) poorly annealed ($T_p = 3.16$) and (d) well-annealed sample ($T_p = 0.04$). The plastic activity is diffuse for PA samples while it is strongly localized inside a band for WA samples. (inset) Row-averaged E_0 profile is plotted with the innermost blue curve at $\gamma = 4.0$ till the outermost red curve at $\gamma = 20.0$ in steps of $\gamma = 4.0$. (e) Bauschinger Effect: The forward and reverse strain response is plotted for a fresh sample (dashed and dotted lines respectively) and a pre-sheared sample (solid lines). Significant anisotropy in forward and reverse response can be observed for the pre-sheared sample. The inset shows the initial loading-unloading curves. (f) The distribution of local distances to strain thresholds is plotted in either direction for the pre-sheared and fresh sample. System size is $L = 512$.

lution towards the absorbing case, followed by a sharp up-jump when a shear band forms and the subsequent evolution involves motion of this shear band which anneals the system further, which explains the dip in energy seen for some cases at large number of cycles. E_0 maps

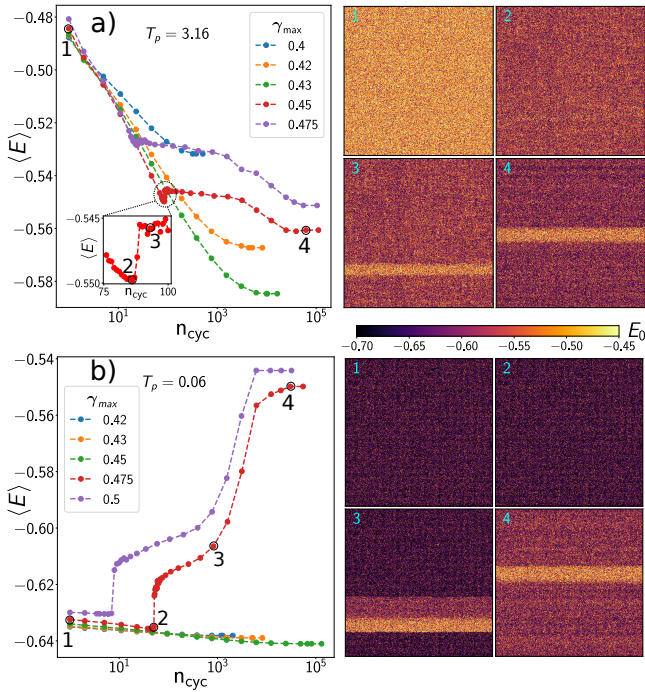


FIG. 3. (a) Per site elastic energy (E) evolution is plotted for (a) poorly annealed sample ($T_p = 3.16$) and (b) well annealed sample ($T_p = 0.06$) for a range of γ_{max} values below and above the yield point. Color-maps of E_0 field for configurations taken at points numbered 1 – 4 are shown to the right of the respective panel.

are plotted on the right hand side, corresponding to configurations taken from points 1 – 4 indicated in Fig. 3a. The higher-energy banded structure is the shear band. In Fig. 3b we repeat the same analysis for a well annealed case ($T_p = 0.06$). For driving amplitudes at and below the critical value of $\gamma_{\text{max}}^{\text{yield}} = 0.475$ an absorbing state is reached with negligible change in the mean energy. At higher γ_{max} initial minimal annealing is followed by a sharp jump that signals the formation of a shear band. Further evolution denotes the shear band movement, moving ballistically [30] till all the sites are visited and then diffusing indefinitely in the solid.

These results are largely consistent with behaviour observed in simulations [22, 25, 33], except for the secondary annealing observed. This appears to be a feature of EPMs (seen also in [30]), but whether it faithfully captures the behaviour of glasses is unclear at present. In similar vein, we find that the yield point is not sharp; a *coexistence* region exists in the vicinity of the yield point where the probability of evolving to an absorbing state drops from 1.0 to 0.0 over a finite range (of typical size 0.02) of driving amplitudes (data shown in [46]). Interestingly, it is difficult to assess, with the available data, whether the width will vanish in the limit $L \rightarrow \infty$ (see [46]), and the significance of this co-existence region remains to be understood by future work.

We define the mid-point of the *coexistence* region to be the yield point and report time-divergence data outside the *coexistence* region. In Fig. 4a we plot the steady state (or absorbing state) stroboscopic energies as a function of driving amplitude for various degrees of annealing. For loading amplitudes till $\gamma_{\text{max}}^{\text{yield}} = 0.43$, all samples reach a stable state where we see complete cessation of plastic activity. Beyond $\gamma_{\text{max}}^{\text{yield}}$ poorly annealed samples exhibit a shear band, and the system reaches a steady (rather than a stable) state. For well annealed samples, the transition occurs at progressively larger γ_{max} values. Above the yield point, all initial conditions trace the same curve implying complete erasure of memory of initial conditions. The initial conditions are erased by way of motion of the shear band which moves throughout the sample. As mentioned, this feature may or may not reflect the corresponding situation in molecular glasses.

In Fig. 4b we plot the number of yield events undergone per site per cycle (yield rate) for a poorly annealed sample. We see a clear non-monotonicity, a reduction in yield events which is abruptly followed by an upturn upon failure, where a steady yield rate is observed, stemming from plastic activity in the shear band. A satisfactory qualitative match can be observed with the analytically derived yield rate reported in [29].

The average time to failure is plotted for a poorly annealed sample ($T_p = 3.16$) in Fig. 4c (orange points), while the same for a well annealed sample ($T_p = 0.04$) is plotted in the inset (orange points). 1000 samples were considered for each driving amplitude and the system size was $L = 128$. A power law behaviour is observed, $\tau_f \propto (\gamma_{\text{max}} - \gamma_{\text{max}}^{\text{yield}})^{-\beta}$, where $\beta = -1.02 \pm 0.02$ for the poorly annealed sample and $\beta = -2.2 \pm 0.1$ for the well-annealed case. Recent 3D particle simulation results [33] observe an exponent of -2 irrespective of annealing level while preliminary results for 2D glasses suggest an exponent of -1 [50]. Mean field investigations [29, 34] present a failure time exponent of -1 for poorly annealed samples and $-1/2$ for well annealed samples. While the lack of agreement with mean field results may be attributable to the approximations involved in those calculations, the deviation from simulation results is puzzling and needs an explanation. The apparent dimensionality dependence may offer an explanation, albeit a surprising one, which will be pursued further in future work. The time to reach an absorbing state for driving amplitudes below the yield point is plotted as green curve in the Fig. 4c. Power-law divergence is observed with exponent -3.2 ± 0.1 , close to what is reported in [19, 26, 31]. A log-divergence was observed instead in [30] which we speculate is the behaviour of the system in the coexistence region.

Contrary to the results and expectation expressed in [22, 30] the present results show that the region outside the shear band does not have an average energy that is independent of the strain amplitude. The yielded state at γ_{max} values close to the transition shows a shear band

diffusing in a background that is *lower* in energy as compared to that for higher γ_{max} values, see Fig. 4d. For larger values of γ_{max} , the average energy outside the shear band appears more constant, but higher than the threshold energy. The shear band width w follows a power law growth as distance from yield amplitude increases, $w/L = w_0/L + A(\gamma_{max} - \gamma_{max}^{yield})^\eta$, see red dotted line in the inset of Fig. 4d, with a non-zero width fraction of about 7.5% at the yield point, and the exponent is 0.73. Following [30, 51, 52] if we enforce that the shear band width should follow a square-root growth law, that is, $w/L = A(\gamma_{max} - \gamma_y)^{1/2}$ where γ_y is a fit parameter, we find $\gamma_y = 0.373 < \gamma_{max}^{yield}$ (see blue dashed line in inset of Fig. 4d; within the quality of the data, these fits are indistinguishable) which also implies that at the yielding transition the shear band has a finite width of around 8%.

Discussion — We have introduced an elasto-plastic model building on the single-site mesostate model introduced in [27]. The model reproduces several aspects of yielding behaviour under uniform and cyclic deformation that have been reported in previous work. These include, for uniform shear, the brittle-to-ductile crossover in yielding behaviour with annealing and the Bauschinger effect. For cyclic shear, the qualitative features of the yielding diagram are reproduced. Poorly annealed glasses exhibit mechanical annealing, and evolve towards a unique threshold energy as the strain amplitude γ_{max} is increased towards a common yield value. Well annealed glasses show negligible annealing before yielding at yield strain amplitudes that depend on, and increase with, the degree of annealing. Failure, upon repeated cycles of shear, is accompanied, close to the yield point, by a non-monotonic evolution of energies and yield rate, and failure times (or below the yield point, cycles to reach absorbing states) exhibit power law divergences at the yield point. In addition these, however, we observe several new features that merit further investigation. The yielded state exhibits further annealing due to the movement of the shear band, that has no analog in simulations of glasses, a feature that further appears to be associated with the region outside the shear bands exhibiting average energies that differ from the threshold energy for different amplitudes, at variance with suggestions from previous work [22, 30]. While power law divergences are observed for failure times, the exponent values do not agree with previous simulations and calculations. Such lack of agreement also leads to the intriguing suggestion that the failure time exponent may be dependent on the spatial dimensionality, which needs to be verified and rationalized. Finally, our results indicate the presence of an intermediate regime around the yield point, in which only a fraction of the samples investigated undergo failure; the width of this regime does not show a convincing reduction to zero as the system size increases. Such a feature, if it persists, is novel, and therefore merits fur-

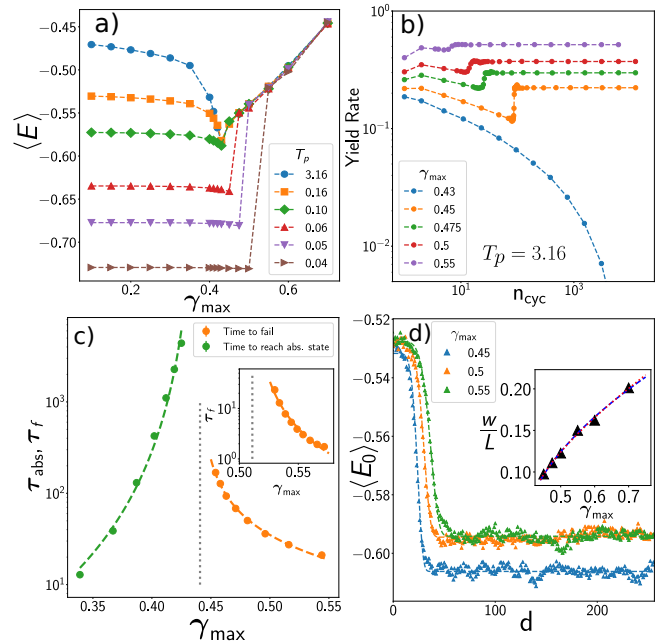


FIG. 4. (a) Steady state energies are plotted at various shear amplitudes for various degrees of annealing (b) Evolution of number of plastic events per site per cycle - the yield rate - is plotted for a poorly annealed sample ($T_p = 3.16$) above and below the yield point $\gamma_{max}^{yield} = 0.43$. (c) Number of cycles to reach an absorbing state (τ_{abs}) and to fail (τ_f) are plotted for a poorly annealed sample. Dashed lines are power-law fits with exponents -3.2 (τ_{abs} , green) and -1.02 (τ_f , orange); vertical line denotes the yield amplitude in the main panel and the inset. (Inset) τ_f is plotted for a well-annealed sample. Dashed line shows a power-law fit with exponent -2.2 . (d) Energy profiles averaged along the direction of the shear band are shown (centered by hand at zero, only the right half is plotted) for a poorly annealed sample ($T_p = 3.16$). Dashed lines are fits to a flat top Gaussian profile $c_1 + c_2 e^{-(x/c_3)^6}$. (Inset) The shear band width is plotted as function of the driving amplitude. Dotted black line is a power law fit $w/L = w_0/L + A(\gamma_{max} - \gamma_{max}^{yield})^{0.73}$. Grey dashed line denotes the fit, $w/L = A(\gamma_{max} - \gamma_y)^{1/2}$, where γ_y is a free parameter, with the fit value being $\gamma_y = 0.363$.

ther study. Although many of the results discussed are generically observed, some features, such as the pinning, *vs.* movement, of the shear bands, depend on the choice of model features in a manner that needs to be understood better. Our work thus demonstrates the need, and paves the way, for future work on designing EPMs that accurately capture the rich phenomenology of amorphous solids.

Acknowledgements: We thank H. Bhaumik, S. Maity, M. Mungan, A. Rosso, D. Sarkar and P. Sollich for useful discussions and comments on the manuscript. S. S. acknowledges SERB(ANRF) (India) for support through the JC Bose Fellowship (JBR/2020/000015) SERB(ANRF), DST (India) and a grant under SUPRA (SPR/2021/000382).

* sastry@jncasr.ac.in

[1] D. Bonn, M. M. Denn, L. Berthier, T. Divoux, and S. Manneville, *Rev. Mod. Phys.* **89**, 035005 (2017).

[2] C. A. Schuh, T. C. Hufnagel, and U. Ramamurty, *Acta Materialia* **55**, 4067 (2007).

[3] S. Bonfanti, R. Busch, J. Byggmästar, J. C. Dyre, J. Eckert, S. Fajardo, M. L. Falk, I. Gallino, J. J. Kružić, J. Lu, G. Monaco, M. Ozawa, A. D. S. Parmar, C. H. Rycroft, and S. Sastry, (2025), arXiv:2512.16590 [cond-mat.mtrl-sci].

[4] A. Argon, *Acta Metallurgica* **27**, 47 (1979).

[5] M. L. Falk and J. S. Langer, *Phys. Rev. E* **57**, 7192 (1998).

[6] D. L. Malandro and D. J. Lacks, *The Journal of Chemical Physics* **110**, 4593 (1999).

[7] J. Pollard and S. M. Fielding, *Phys. Rev. Res.* **4**, 043037 (2022).

[8] L. Berthier, G. Biroli, L. Manning, and F. Zamponi, *Nature Reviews Physics* **7**, 313 (2025).

[9] T. Divoux, C. Barentin, and S. Manneville, *Soft Matter* **7**, 9335 (2011).

[10] Y. Shi and M. L. Falk, *Phys. Rev. Lett.* **95**, 095502 (2005).

[11] M. Fan, M. Wang, K. Zhang, Y. Liu, J. Schroers, M. D. Shattuck, and C. S. O'Hern, *Phys. Rev. E* **95**, 022611 (2017).

[12] M. Ozawa, L. Berthier, G. Biroli, A. Rosso, and G. Tarjus, *Proceedings of the National Academy of Sciences* **115**, 6656 (2018).

[13] T. Mukai, T. Nieh, Y. Kawamura, A. Inoue, and K. Higashi, *Intermetallics* **10**, 1071 (2002).

[14] F. Varnik, L. Bocquet, J.-L. Barrat, and L. Berthier, *Phys. Rev. Lett.* **90**, 095702 (2003).

[15] M. Singh, M. Ozawa, and L. Berthier, *Phys. Rev. Mater.* **4**, 025603 (2020).

[16] H. J. Barlow, J. O. Cochran, and S. M. Fielding, *Phys. Rev. Lett.* **125**, 168003 (2020).

[17] N. V. Priezjev, *Phys. Rev. E* **87**, 052302 (2013).

[18] D. Fiocco, G. Foffi, and S. Sastry, *Phys. Rev. E* **88**, 020301 (2013).

[19] I. Regev, T. Lookman, and C. Reichhardt, *Phys. Rev. E* **88**, 062401 (2013).

[20] T. Kawasaki and L. Berthier, *Phys. Rev. E* **94**, 022615 (2016).

[21] P. Leishangthem, A. D. S. Parmar, and S. Sastry, *Nature Communications* **8**, 14653 (2017).

[22] A. D. S. Parmar, S. Kumar, and S. Sastry, *Phys. Rev. X* **9**, 021018 (2019).

[23] W. T. Yeh, M. Ozawa, K. Miyazaki, T. Kawasaki, and L. Berthier, *Phys. Rev. Lett.* **124**, 225502 (2020).

[24] P. Das, H. A. Vinutha, and S. Sastry, *Proceedings of the National Academy of Sciences* **117**, 10203 (2020).

[25] H. Bhaumik, G. Foffi, and S. Sastry, *Proceedings of the National Academy of Sciences* **118**, e2100227118 (2021).

[26] K. Khirallah, B. Tyukodi, D. Vandembroucq, and C. E. Maloney, *Phys. Rev. Lett.* **126**, 218005 (2021).

[27] S. Sastry, *Phys. Rev. Lett.* **126**, 255501 (2021).

[28] M. Mungan and S. Sastry, *Phys. Rev. Lett.* **127**, 248002 (2021).

[29] J. T. Parley, S. Sastry, and P. Sollich, *Phys. Rev. Lett.* **128**, 198001 (2022).

[30] C. Liu, E. E. Ferrero, E. A. Jagla, K. Martens, A. Rosso, and L. Talon, *The Journal of Chemical Physics* **156**, 104902 (2022).

[31] D. Kumar, S. Patinet, C. E. Maloney, I. Regev, D. Vandembroucq, and M. Mungan, *The Journal of Chemical Physics* **157**, 174504 (2022).

[32] J. O. Cochran, G. L. Callaghan, M. J. G. Caven, and S. M. Fielding, *Phys. Rev. Lett.* **132**, 168202 (2024).

[33] S. Maity, H. Bhaumik, S. Athani, and S. Sastry, (2024), arXiv:2409.17384 [cond-mat.soft].

[34] D. Sarkar, J. N. Nampoothiri, M. Mungan, J. T. Parley, P. Sollich, and S. Sastry, (2025), arXiv:2505.14912 [cond-mat.stat-mech].

[35] A. Nicolas, E. E. Ferrero, K. Martens, and J.-L. Barrat, *Rev. Mod. Phys.* **90**, 045006 (2018).

[36] P. Sollich, F. m. c. Lequeux, P. Hébraud, and M. E. Cates, *Phys. Rev. Lett.* **78**, 2020 (1997).

[37] E. Agoritsas, E. Bertin, K. Martens, and J.-L. Barrat, *The European Physical Journal E* **38**, 71 (2015).

[38] M. Mungan, S. Sastry, K. Dahmen, and I. Regev, *Phys. Rev. Lett.* **123**, 178002 (2019).

[39] R. Chatterjee, M. Adhikari, and S. Karmakar, (2024), arXiv:2403.16972 [cond-mat.soft].

[40] A. Nicolas, F. Puosi, H. Mizuno, and J.-L. Barrat, *Journal of The Mechanics and Physics of Solids* **78**, 333 (2015).

[41] S. Sandfeld, Z. Budrikis, S. Zapperi, and D. F. Castellanos, *Journal of Statistical Mechanics: Theory and Experiment* **2015**, P02011 (2015).

[42] G. Picard, A. Ajdari, F. Lequeux, and L. Bocquet, *The European Physical Journal E* **15**, 371 (2004).

[43] M. Talamali, V. Petäjä, D. Vandembroucq, and S. Roux, *Comptes Rendus Mécanique* **340**, 275 (2012), *recent Advances in Micromechanics of Materials*.

[44] E. A. Jagla, *Phys. Rev. E* **76**, 046119 (2007).

[45] X. Cao, A. Nicolas, D. Trimcev, and A. Rosso, *Soft Matter* **14**, 3640 (2018).

[46] P. Khandare and S. Sastry, Supplemental Material to be included, for details on the finite element method implementation, sample preparation, shear band growth under uniform shear, determination of cyclic shear yield point, fatigue failure, effect of model parameters on the yielding transition and trenching, and includes references [27, 40? ? ? ?].

[47] S. Karmakar, E. Lerner, and I. Procaccia, *Phys. Rev. E* **82**, 026104 (2010).

[48] N. C. Keim, J. D. Paulsen, Z. Zeravcic, S. Sastry, and S. R. Nagel, *Rev. Mod. Phys.* **91**, 035002 (2019).

[49] S. Patinet, A. Barbot, M. Lerbinger, D. Vandembroucq, and A. Lemaître, *Phys. Rev. Lett.* **124**, 205503 (2020).

[50] H. Bhaumik, personal communication.

[51] E. A. Jagla, *Journal of Statistical Mechanics: Theory and Experiment* **2010**, P12025 (2010).

[52] D. D. Alix-Williams and M. L. Falk, *Phys. Rev. E* **98**, 053002 (2018).